An Optimized Measurement Algorithm for Gas Sensors Based on Carbon Nanotubes: Optimizing Sensor Performance and Hardware Resources

Encarnación Castillo, José F. Salmerón, Aniello Falco, Florin C. Loghin, Francisco J. Romero, Paolo Lugli, Diego P. Morales⁣, and Almudena Rivadeneyra⁣

Abstract—This paper presents a novel algorithm for the measurement of resistive-type gas sensors with carbon nanotubes (CNTs) as sensitive layer. Contrary to conventional strategies, which extract the sensor information from the normalized resistance, the proposed algorithm is based on the variation in resistance over time. The results have demonstrated that the time necessary to get the maximum performance of these sensors is reduced around a 25% when compared with the conventional approach for any of the recovery strategies analyzed (passive desorption, external heating, or dc voltage). The hardware implementation of the proposed algorithm in a field-programmable gate array (FPGA) has also demonstrated that, in addition to optimizing the sensor performance in terms of time response and sensitivity, this measurement algorithm yields a significant minimization of the sensor readout circuit resources at both software and hardware levels paving the way for future development of smart sensors for the Internet of Things (IoT) applications.

Index Terms—Carbon nanotube (CNT), field-programmable gate array (FPGA), inkjet printing, NH_3, recovery, single-walled, spray deposition.

I. INTRODUCTION

RECENTLY, gas leakage detection is a topic of high interest in diverse fields from personal to industrial applications. In this context, thanks to the rapid advances in the development of wireless sensors devices into the Internet of Things (IoT) paradigm, there is a current trend toward ubiquitous sensing. However, significant challenges remain concerning the widespread availability of this kind of devices for end-user applications. On the one hand, sensors need to be lightweight, low-power, robust, and small in size and, on the other hand, the algorithms implemented in the IoT devices must be optimized to minimize both computing resources and time, and consequently, the power consumption.

Therefore, it is clear that the convergence between nanotechnology (new materials and detection methods, manufacturing processes, device integration, etc.) and both measuring and processing algorithms is mandatory to move forward in this effort [1].

Regarding gas sensors, resistive ones are very popular because of their reasonable price and good durability [2]. However, they are commonly limited in their selectivity and sensitivity, boosting research to develop new materials and detection methods for a better gas discrimination [3]. In this direction, functional materials have received a lot of attention. A large variety of electrical sensor materials have been investigated, including semiconducting metal oxides, silicon devices, organic materials, carbon nanotubes (CNTs) and carbon black-polymer composites [4]. These new materials are normally tuned by functionalizing them with metal and polymers to achieve selectivity toward certain gas species [5]; however, the vast majority of the solutions are time and power demanding. Therefore, several approaches have been developed toward facing these issues, for instance, higher-order sensing systems which consist of sensor arrays covered with different sensitive layers [6], using pattern recognition algorithms [7], or multifunctional sensors which measure different properties of a sensitive layer [8]. Furthermore, it is desirable to recover the sensor response over time, that is to say, to desorb the trapped molecules in the sensing element after being exposed to the gas. A common strategy to recover the sensing layer is to externally heat the sensor to increase the desorption rate of the trapped molecules [9]–[11]. This approach normally requires the integration of more circuitry and higher power consumption. Recently, we have reported the capability of CNTs gas sensors to self-recover by applying a higher than probing dc voltage between its terminals, reducing the power demand of the system as well as not requiring more circuit elements for the recovery stage [12]. A lot of effort has been put in developing this kind of gas sensor because they present high sensitivity toward a variety of gas species [5], [13], [14], can be manufactured with cost-effective techniques [15], [16] and can be deposited on flexible substrates [17], [18], providing a promising starting point for the industrial use of this technology. However, very limited attention has been paid to their transduction mechanisms in terms of the requirements to be integrated at system level.

Conventionally, the information of resistive sensors is extracted from their normalized resistance (NR). In other words, it is measured the relative change in resistance when the sensor is exposed to the parameter of interest with respect to its value under base level conditions [10], [19], [20]. One essential part of any sensory system, mostly neglected by basic research, is the integration of the sensing element in a complete electronic system. This requires the design of circuits to adapt the sensor signal and efficiently and accurately extract the sensor information [21].

In this paper, we propose a new algorithm to analyze the response of a CNT gas sensor based on its relative change of resistance over time and we demonstrate its superiority over the NR, the conventional approach, at the sensor performance and at the employed hardware resources for extracting information. We investigate this novel approach in terms of time response, sensitivity, and level of integration in final systems. One of the most desirable aspects in the field of instrumentation is to bring the intelligence to the sensor elements through the applications of low computational cost, small size, and low consumption. Thus, the measurement algorithm proposed in this paper allows optimizing the resources of implementation and computation, making feasible the future development of a smart sensor, crucial for the truly development of the paradigm of the IoT.

This paper is organized as follows. In Section II, the design and fabrication of the sensor is described together with its characterization procedure. Section III describes the proposed algorithm and presents its empirical results in comparison with the conventional method. At the end of this section, it is analyzed the system requirements of each approach and their feasibility of circuitry integration. Finally, the main conclusions are drawn in Section IV.

II. Materials and Methods

A. Fabrication Process

Initially, we sprayed the CNT solution on the polyimide substrate (Kapton HN) of 125 μm-thickness. The CNTs were dispersed in an aqueous solution based on 1 wt.% sodium dodecyl sulfate (SDS). After stirring the solution for 1 h, 0.03 wt.% CNTs were added to the dissolved dispersion agent. The obtained solution was sonicated for 30 min using horn sonicator at 50% of its maximum power ($\sim$48 W). After 1.5 h of centrifugation at 15 000 rpm, the top part of the solutions was removed from the vials to be used for the deposition, while the bottom 20% was disposed. By mounting an air atomizing spray valve (Nordson EFD, USA), to a motorized X–Y platform (Precision Valve & Automation, USA), it was possible to obtain a repeatable spray process, using an approach similar to what previously reported [17], [18]. After deposition, the samples were immersed in deionized water for 15 min at room temperature to remove the dispersant, and subsequently dried.

Then, on top of the CNT film, we defined the electrodes, using a DMP-2831 Dimatix printer (Fujifilm Dimatix, Inc., Santa Clara, CA, USA) fixing the plate temperature during printing at 60 °C. The electrodes were made of one layer of silver nanoparticles (DGP 40LT-15C from ANP Company, USA),
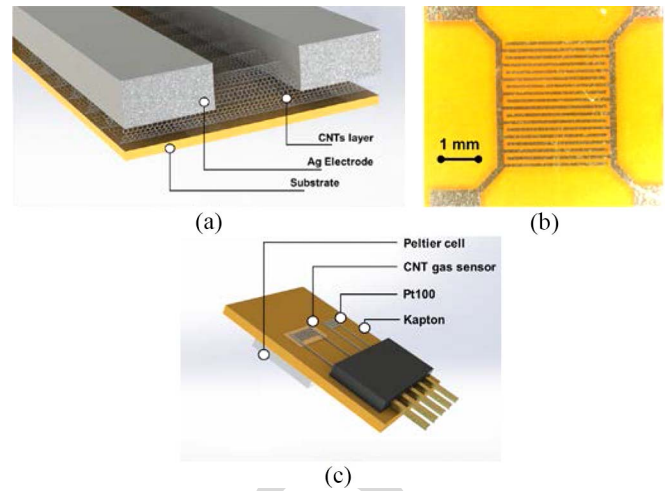
Fig. 1. (a) Schematics of the fabricated sensors. (b) Real picture of the sensor. (c) Schematic of sensor module.

defining the drop space to 50 μm. The finger width and the space between fingers are 100 μm and the finger length 3 mm. After printing and drying of the electrodes, they were photonic sintered (Sinteron 2010 from Xenon, USA) with five pulses of 2.5 kV energy and 500 μs width. Fig. 1(a) illustrates the layers of the manufactured device and Fig. 1(b) presents a real picture of the developed sensor.

The complete sensor module includes the resistive sensor, mounted on a carrier glass together with a Peltier heating element for temperature control and a temperature sensor (Pt100) for *in-situ* monitoring [Fig. 1(c)].

B. Characterization Process

Sensors were measured by monitoring the variation in resistance with respect to the test gas concentration. Before the sensor response toward test gas was analyzed, the initial resistance of the sensor was monitored over time to determine its baseline. After reaching a stable initial value, the sensor module was introduced inside a gas chamber and its response was evaluated by exposing it to different concentrations of test gas. Fig. 2 illustrates a measurement cycle, which is composed of an exposure interval followed by a recovery interval and then an interval at normal conditions. The room temperature was set to *circa* 22°, and in each stage, nitrogen was employed as carrier gas to be certain that the measurement result would only be influenced by the target gas. In "normal conditions" phases, the carrier gas flow was set to 200 ml/min. During exposure phases, the overall mixture flux was set to a constant 200 ml/min for a given time at ambient temperature [stage (c) in Fig. 2].

Recovery was then introduced, following three different strategies [stage (b) in Fig. 2]: 1) externally heating the sensor, with a Peltier cell, to 80 °C; 2) applying 10 V among the sensor terminals to establish a self-heating condition; and 3) passive recovery (leaving the sensor under ambient conditions). For ease of comparison, every recovery strategy was tested with the same conditions (unchanged room temperature, 200 ml/min flux of carrier gas). After these recovery
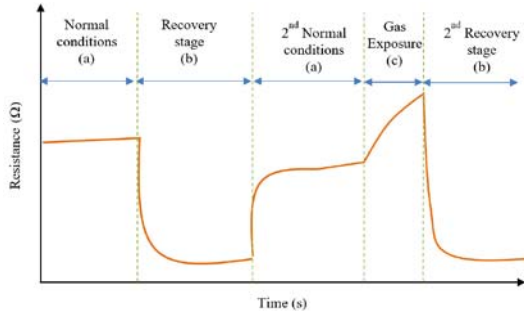
Fig. 2. Schematic of the measurement flow, pointing out the different stages. (a) Operation at normal conditions. (b) Recovery step. (c) Exposure to gas.

phases, the high flux was kept once more at ambient conditions [stage (a) in Fig. 2] to facilitate the recuperation of the device and purge any residual test gas molecules out of the gas chamber. Recovery stage ended by a final step under sensing conditions (200 ml/min of carrier gas at ambient conditions) to help restore the initial resistance before the next exposure cycle. We performed two different measurement tests, a longer one where all the steps in the cycle had a duration of 300 s and a shorter one with the duration of the steps fixed at 150 s.

The measurements were automated with LabVIEW 2016 software, which controlled an impedance analyzer (Keysight E4990A) with an impedance probe kit (4294A1) for the sensor readout (impedance). The excitation voltage applied in all measurements was $V_{dc} = 0$ and $V_{ac} = 500$ mV and the frequency swept ranged from 20 to 100 Hz. The dc voltage to perform the recovery stage was directly applied by the impedance analyzer. The phase in all frequencies was below 10^{-30}, proving the virtually pure resistive behavior of the device under test. In particular, the NH_3 concentrations tested covered a range between 10 and 80 ppm, achieved by diluting the test gas with nitrogen as carrier gas.

III. RESULTS AND DISCUSSION

In this section, we will first show the analysis of the described sensor using the proposed measurement methods and comparing its performance with the conventional procedure. After that, we will show the influence of the recovery strategy in this new measurement protocol, followed by the use of this protocol to the response of the sensor toward other gases. Finally, we will show a study of the efficiency of the described measurement protocol in comparison with the conventional one in hardware and software final solutions.

In the following sections, we present the mean values of three complete measurements cycles. The errors are lower than 2% in all cases.

A. Response to Ammonia

In order to evaluate the sensor performance, the conventional measurement protocol is based on the NR presented in (1): the difference in resistance before and after the exposure divided by this initial resistance. What we propose is to fix the measurement time and only measure the variation in resistance in the chosen time slot, see (2)

$$\text{Normalized Resistance}(\%) = \frac{R_f - R_i}{R_i} \quad (1)$$

$$\text{Temporal Resistance Variation}\left(\frac{\Omega}{s}\right) = \frac{R_f - R_i}{T} \quad (2)$$

where R_i and R_f are the initial and final resistance values of an exposure cycle, respectively, and T is the reference time interval. Notice that once that after the calibration, an optimal value of T will be found, it shall be considered as constant. On the contrary, looking to (1), the initial resistance of the CNT film cannot be considered as constant, since the baseline value is not necessarily recovered after exposure.

The time response of such gas sensing systems is traditionally modeled as a "charging" circuit, with a classic growing negative exponential response [22]

$$R(t) = R_i + \Delta R(C)\left(1 - e^{-\frac{t}{\tau}}\right) \quad (3)$$

$$R'(t) = \frac{\Delta R(C)}{\tau} e^{-\frac{t}{\tau}} \quad (4)$$

$$NR' = \frac{\Delta R(C)}{R_i \tau} e^{-\frac{t}{\tau}}. \quad (5)$$

The derivative of the time evolution of resistance—and, hence, the NR—after exposure is always strictly positive, as presented in (4) and (6), respectively. This implies that the NR will have an increasing value until the slope will be only marginally increased, and saturation can be considered reached. The saturation point, however, could be substantially different, depending on the network properties. The proposed characterization feature, on the other hand, focuses on the temporal resistance variation (TRV), introduced in the previous section. The TRV will quickly reach its maximum and then decrease over time, toward a more stable value. Proceeding similar to what we did for the NR, it is possible to write TRV and its derivative as

$$\text{TRV}(t) = \frac{\Delta R(C)}{t}\left(1 - e^{-\frac{t}{\tau}}\right) \quad (6)$$

$$\text{TRV}'(t) = -\frac{\Delta R(C)}{t^2}\left(1 - e^{-\frac{t}{\tau}}\right) + \frac{\Delta R(C)}{t\tau} e^{-\frac{t}{\tau}}. \quad (7)$$

Thus, the derivative with respect to time of TRV is strictly negative and quickly approaching zero. The maximum of the TRV response will be observed immediately after exposure.

Fig. 3(a) and (b) shows the NR while the sensor is exposed to the test gas, whereas Fig. 3(c) and (d) presents the TRV during the test gas exposure. In particular, Fig. 3(a) and (c) corresponds to 150 s exposure while Fig. 3(b) and (d) to 300 s. It can be observed how the shapes of the curves are independent on the exposure time. In the case of the NR, the sensor has not achieved the saturation point. If the exposure takes longer, it is expected to have an increase in the NR and, therefore, the response of the sensor would be higher, the longer the exposure is. Contrary to this behavior, the TRV depicts a faster increase in its response around the first 50 s exposure and it tends to a constant value above 120 s. This response provides us a new resource to characterize this sensor, ensuring a stable value and, especially, facilitating its integration in final systems.
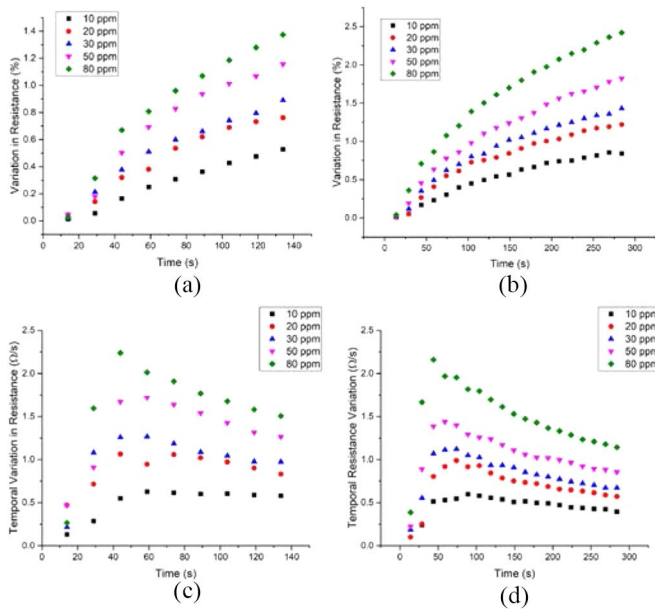
Fig. 3. NR over time for different NH_3 concentrations with an exposure time of (a) 150 s and (b) 300 s. TRV over time at the same NH_3 concentrations with an exposure time of (c) 150 s and (d) 300 s.
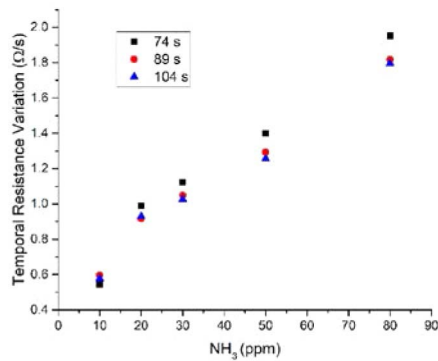
Fig. 4. Temporal resistance variation versus ammonia concentration at different exposure times.

The calibration curve of the sensor considering the TRV over NH_3 concentration is illustrated in Fig. 4, selecting three different point of time. At 74 s, the response is slightly higher than at longer time exposure. Contrary to the traditional measurement (NR), longer exposure time does not ensure a better response of the sensor.

Basically, when using NR, the response achieves its maximum at saturation and to reach this point we have to wait until the resistance stabilizes (meaning in this case, a time longer than 300 s). Opposite to this approach, when applying TRV, how fast the resistance changes with the concentration exhibits an increase at the beginning until reach a maximum (in this case, about 75 s) and then stabilized.

The linear regression curves extracted from data in Fig. 4 are presented in (8)–(10) for 74, 89, and 104 s, respectively

$$\text{TVR}(\Omega/s) = 0.01844 \cdot [NH_3] + 0.50105, R^2 = 0.95138 \quad (8)$$

$$\text{TVR}(\Omega/s) = 0.01631 \cdot [NH_3] + 0.51455, R^2 = 0.97501 \quad (9)$$

$$\text{TVR}(\Omega/s) = 0.01603 \cdot [NH_3] + 0.50833, R^2 = 0.96319. \quad (10)$$

Notice an important improvement that TRV achieves compared to the NR for the integration of the sensing element in a complete electronic system. For the computation of the NR it can be observed that (1) includes a division to an arbitrary real number (the measured initial resistance value). This arithmetic operation, albeit important, is far more complex than addition and multiplication, and requires significant amount of resources for a complete hardware implementation [23], [24]. Thus, a challenge, sometimes difficult to achieve, is to be able to manipulate the algebraic expression in order to convert it into another one that only includes multiplications and/or additions. Achieving the above would make it possible to get an area reduction and performance improvement of the hardware implementation, a very important aspect to be able to provide a competitive portable design. In this sense, for the computation of the TRV, (2) matches the requirements of the previous challenge, since the term T is a constant value, statically chosen in design phase, and the division by this constant can be easily converted into a multiplication [25]. Thus, in addition to the advantage related to the faster increase in its response, the TRV facilities the integration in final systems.

Similar results have been found for ethanol (see Fig. S1), demonstrating the wider use of the proposed algorithm.

Muezzinoglu [26] also proposed an analysis of the transient response of chemo-resistive sensors providing a faster response without waiting until the sensor achieve the equilibrium point. However, in their approach, it is needed to employ various multiplications; while, in our algorithm, only one simple multiplication is needed. Moreover, contrary to them, we demonstrate that no data transformation is needed to extract the sensor information.

B. Response Using Different Recovery Strategies

The recovery of the sensor to its baseline after finishing the exposure to the gas is an important feature of any gas sensor, although the vast majority does not completely recover to their baseline but they show substantial drifts after different exposure cycles [27], [28]. SWNT gas sensors are one of those devices that do not recuperate the baseline at ambient conditions after exposure to a test gas [29]. In order to force the sensor to recover its initial characteristics, it is necessary to provide extra energy in the form of heat or gate biasing or UV light [29]–[32]. The data presented in Figs. 3 and 4 corresponds to a recovery strategy based on external heating (in this case, at 80 °C), as this is the most established approach. Nevertheless, recently it has been proved that a similar effect can be achieved by applying a dc voltage [12]. Even in this case, however, the power demand of the sensing system is significantly higher than what a simple resistance measurement would require. Resultantly, an even more remarkable finding would be to avoid the recovery to the baseline, leaving the sensor to passively get rid of the trapped molecules (passive recovery), and still be able to guarantee high and repeatable response.

Fig. 5 shows the analysis presented in the previous section for dc voltage recovery [Fig. 5(a) and (b)] and for passive recovery [Fig. 5(c) and (d)]. The shapes obtained are similar
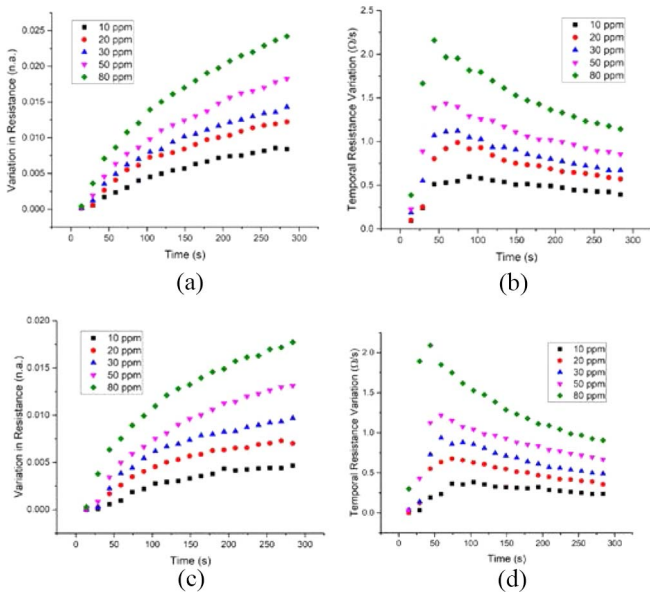
Fig. 5. (a) NR over time for different NH_3 concentrations with an exposure time of 300 s and recovery at 10 V. (b) TRV over time at the same NH_3 concentrations with an exposure time of 300 s and recovery at 10 V. (c) NR over time for different NH_3 concentrations with an exposure time of 300 s and passive recovery. (d) TRV over time at the same NH_3 concentrations with an exposure time of 300 s and passive recovery.

to the external heating recovery for both NR and TRV. When we look at the NR, the active recovery strategies (heating at 80 °C and applying 10 V) achieve around 2.5% at 80 ppm NH_3 after 300 s, while the response is below 2% for passive recovery at the same concentration and point of time. But when we look at the TRV, this difference is reduced. For example, we measured 1.9 Ω/s at 80 ppm NH_3 and 74 s for heating recovery, 2.0 Ω/s for dc voltage recovery, and 1.8 Ω/s for passive recovery. Hence, the response loss with respect to the active recovery case is 18% and 5% for the NR and TRV methods, respectively.

C. Performance in Real Measurement Instrument

Hardware implementation in field-programmable gate array (FPGA) of NR and the new proposal based on TRV have been evaluated and compared. Fig. 6 shows the block diagram of TRV implementation that is based on a finite-state machine (FSM) implementation. VHDL descriptions of the developed designs have been implemented using Spartan 6 xc6vlx40t-1fgg1156 [33] and Cyclone II EP2C20F484C7 [34] devices from Xilinx and Intel (formerly, Altera), respectively. The architectures have been designed for two different exposure times, 128 and 256 s. These exposure times are within the range of interest and have been selected since to divide by a power of 2 using binary representation is equivalent to displacements to the right of the data record, thus reducing the required area resources. In order to get these exposure times, the designs were developed taking into account the frequencies of the clock sources coming into the FPGA devices. 200 and 50 MHz clock sources were used for Spartan 6 and Cyclone II devices, respectively.
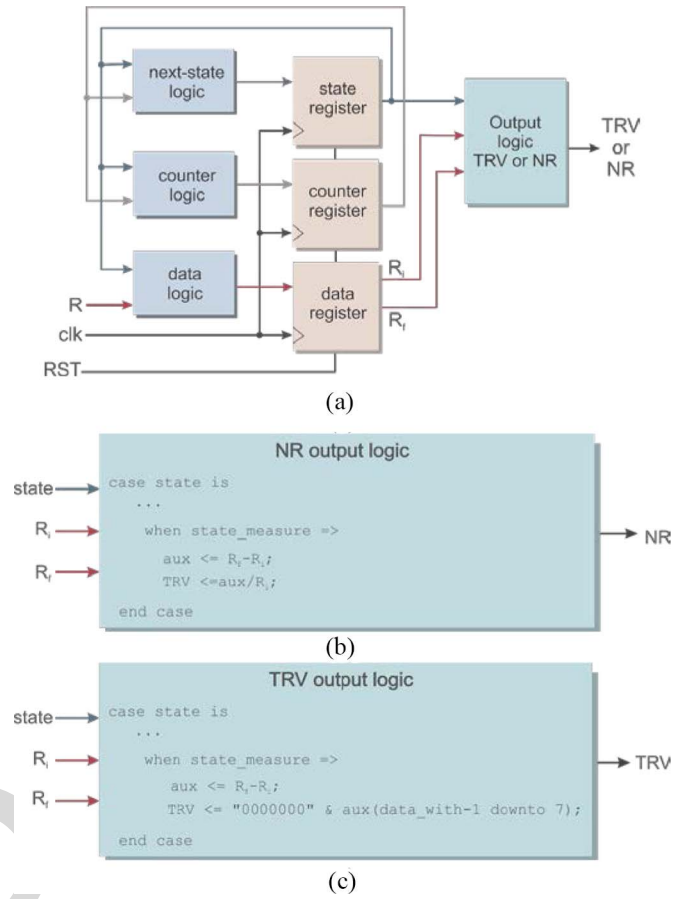
Fig. 6. (a) Block diagram of TRV or NR algorithm implemented in FPGA. (b) VHDL sentences for NR output logic for NR algorithm. (c) VHDL sentences for TRV output logic (for an exposure time of 128 s).

TABLE I
AREA AND DELAY FIGURES FOR FPGA IMPLEMENTATION
USING AN EXPOSURE TIME OF 128 S

| Design | Spartan 6 | | | |
	Area (Slices)	Ratio	F_{max} (MHz)	Ratio
NR	99	1	29.49	1
TRV	25	0.25	478.87	0.06
Design	Cyclone II			
	Area (LEs)	Ratio	F_{max} (MHz)	Ratio
NR	374	1	20.27	1
TRV	83	0.22	189.04	0.11

Tables I and II summarize the area and maximum frequency figures for these FPGA implementations. It can be observed from these tables that TRV design occupies a much smaller area than NR design. Concretely, TRV design occupies around 75% less area than NR for both exposure times and FPGA devices. In addition to this, the high surface and the more complex structures lower significantly the operating frequency of the circuits. These tables also show how the NR designs in the Spartan 6 and Cyclone II fall short of the reference frequencies of 200 and 50 MHz. For instance, in case of the Spartan 6, the maximum frequency stops at

TABLE II
AREA AND DELAY FIGURES FOR FPGA IMPLEMENTATION
USING AN EXPOSURE TIME OF 256 S

Spartan 6				
Design	Area (Slices)	Ratio	F_{max} (MHz)	Ratio
NR	101	1	30.25	1
TRV	27	0.27	327.44	0.09
Cyclone II				
Design	Area (LEs)	Ratio	F_{max} (MHz)	Ratio
NR	377	1	20.07	1
TRV	86	0.23	199.20	0.11

29.29 and 30.25 MHz for an exposure time of 128 and 256 s, respectively. A similar situation occurs for Cyclone II devices and NR designs. To effectively use these circuits, a clock divider component should be implemented, increasing thus the area resources. In this sense, TRV designs substantially improve the maximum frequency, increasing around a 90% the maximum frequencies. For example, the maximum frequencies supported by TRV designs for Spartan 6 device are 478.87 and 327.44 MHz for an exposure time of 128 and 256 s, respectively, which satisfy the required frequency of 200 MHz. As a result, TRV designs in addition to reduce area occupation, allow reaching the required frequencies, without being necessary to include a clock divider component, which further increase the complexity.

IV. CONCLUSION

This paper proposes and develops a novel measurement algorithm for gas sensors based on single-walled CNTs. This algorithm not only optimizes the sensor performance in terms of time response and sensitivity but also facilitates the integration of the sensor in a final system, minimizing hardware resources, and power consumption.

The described algorithm is based on the measurement of the variation in resistance over time, what we define as time resistance variation (TRV). We demonstrate that only 74 s are necessary to get the maximum performance of the sensor response for ammonia detection and this value is applicable for different recovery strategies (passive desorption, external heating, and dc voltage). In the case of the conventional approach, measuring the NR does not get the best performance below 300 s for any of the recovery strategies analyzed. Although both calculations of TRV and NR involve a division, the practical computation of TRV can be reduced by a subtraction of two resistance values whereas the division in NR cannot be simplified, because the initial resistance changes over time. Therefore, from a computational point of view and in terms of circuit resources, TRV results in a faster solution, requiring a minimal number of electronic blocks for the hardware implementation to extract the sensor information. Thus, the hardware implementation in FPGA of NR and TRV designs has demonstrated that TRV design reduces the area resources and increases substantially the operating frequency.

REFERENCES

[1] F. V. Paulovich, M. C. F. De Oliveira, and O. N. Oliveira, "A future with ubiquitous sensing and intelligent systems," *ACS Sensors*, vol. 3, no. 8, pp. 1433–1438, Aug. 2018.

[2] G. Sberveglieri, "Recent developments in semiconducting thin-film gas sensors," *Sensors Actuators B Chem.*, vol. 23, nos. 2–3, pp. 103–109, Feb. 1995.

[3] J. M. Smulko *et al.*, "New approaches for improving selectivity and sensitivity of resistive gas sensors: A review," *Sensor Rev.*, vol. 35, no. 4, pp. 340–347, Apr. 2015.

[4] K. Arshak, E. Moore, G. M. Lyons, J. Harris, and S. Clifford, "A review of gas sensors employed in electronic nose applications," *Sensor Rev.*, vol. 24, no. 2, pp. 181–198, 2004.

[5] K. Balasubramanian and M. Burghard, "Chemically functionalized carbon nanotubes," *Small*, vol. 1, no. 2, pp. 180–192, Dec. 2004.

[6] C. Hagleitner *et al.*, "Smart single-chip gas sensor microsystem," *Nature*, vol. 414, pp. 293–296, Nov. 2001.

[7] F. Hossein-Babaei, S. M. Hosseini-Golgoo, and A. Amini, "Extracting discriminative information from the Padé-Z-transformed responses of a temperature-modulated chemoresistive sensor for gas recognition," *Sensors Actuators B Chem.*, vol. 142, no. 1, pp. 19–27, Oct. 2009.

[8] J. A. Covington, S. L. Tan, J. W. Gardner, A. Hamilton, T. Koickal, and T. Pearce, "Combined smart chemFET/resistive sensor array," in *Proc. IEEE SENSORS*, 2003, pp. 1120–1123.

[9] D. Vincenzi, "Development of a low-power thick-film gas sensor deposited by screen-printing technique onto a micromachined hotplate," *Sensors Actuators B Chem.*, vol. 77, nos. 1–2, pp. 95–99, Jun. 2001.

[10] K. H. Crowley *et al.*, "Fabrication of an ammonia gas sensor using inkjet-printed polyaniline nanoparticles," *Talanta*, vol. 77, no. 2, pp. 710–717, 2008.

[11] E. Danesh *et al.*, "Development of a new generation of Ammonia sensors on printed polymeric hotplates," *Anal. Chem.*, vol. 86, no. 18, pp. 8951–8958, Aug. 2014.

[12] A. Falco, A. Rivadeneyra, F. C. Loghin, J. F. Salmeron, P. Lugli, and A. Abdelhalim, "Towards low-power electronics: Self-recovering and flexible gas sensors," *J. Mater. Chem. A*, vol. 6, pp. 7107–7113, Mar. 2018.

[13] A. Abdellah, A. Yaqub, C. Ferrari, B. Fabel, P. Lugli, and G. Scarpa, "Spray deposition of highly uniform CNT films and their application in gas sensing," in *Proc. 11th IEEE Int. Conf. Nanotechnol.*, 2011, pp. 1118–1123.

[14] E. Contes-de Jesus, J. Li, and C. R. Cabrera, "Latest advances in modified/functionalized carbon nanotube- based gas sensors," in *Syntheses and Applications of Carbon Nanotubes and Their Composites*. London, U.K.: IntechOpen, 2013, pp. 337–366.

[15] A. Abdelhalim, A. Abdellah, G. Scarpa, and P. Lugli, "Fabrication of carbon nanotube thin films on flexible substrates by spray deposition and transfer printing," *Carbon*, vol. 61, pp. 72–79, Sep. 2013.

[16] A. Abdelhalim, M. Winkler, F. Loghin, C. Zeiser, P. Lugli, and A. Abdellah, "Highly sensitive and selective carbon nanotube-based gas sensor arrays functionalized with different metallic nanoparticles," *Sensors Actuators B Chem.*, vol. 220, pp. 1288–1296, Dec. 2015.

[17] A. Abdellah *et al.*, "Flexible carbon nanotube based gas sensors fabricated by large-scale spray deposition," *IEEE Sensors J.*, vol. 13, no. 10, pp. 4014–4021, Oct. 2013.

[18] A. Abdelhalim, A. Falco, F. Loghin, P. Lugli, J. F. Salmerón, and A. Rivadeneyra, "Flexible NH3 sensor based on spray deposition and inkjet printing," in *Proc. IEEE SENSORS*, 2016, pp. 1–3.

[19] S. Claramunt *et al.*, "Flexible gas sensor array with an embedded heater based on metal decorated carbon nanofibres," *Sensors Actuators B Chem.*, vol. 187, pp. 401–406, Oct. 2013.

[20] G. P. Evans, D. J. Buckley, N. T. Skipper, and I. P. Parkin, "Single-walled carbon nanotube composite inks for printed gas sensors: Enhanced detection of NO2, NH3, EtOH and acetone," *RSC Adv.*, vol. 4, pp. 51395–51403, Oct. 2014.

[21] J. H.-L. Lu and B. Jung, "Sensor conditioning circuits," in *Integrated Circuits for Analog Signal Processing*. New York, NY, USA: Springer, 2013, pp. 223–242.

[22] C. K. Alexander and M. N. O. Sadiku, *Fundamentals of Electric Circuits*. Boston, MA, USA: McGraw-Hill, 2009.

[23] P. Soderquist and M. Leeser, "An area/performance comparison of subtractive and multiplicative divide/square root implementations," in *Proc. 12th IEEE Symp. Comput. Arithmetic*, 1995, pp. 132–139.

[24] T. Drane, W.-C. Cheung, and G. A. Constantinides, "Correctly rounded constant integer division via multiply-add," in *Proc. IEEE Int. Symp. Circuits Syst.*, 2012, pp. 1243–1246.

[25] H. F. Ugurdag, A. Bayram, V. E. Levent, and S. Gören, "Efficient combinational circuits for division by small integer constants," in *Proc. IEEE 23rd Symp. Comput. Arithmetic (ARITH)*, 2016, pp. 1–7.

[26] M. K. Muezzinoglu, "Acceleration of chemo-sensory information processing using transient features," *Sensors Actuators B Chem.*, vol. 137, no. 2, pp. 507–512, Apr. 2009.

[27] D. Kumar, "Investigation of single wall nanotube gas sensor recovery behavior in the presence of UV," *Adv. Mater. Lett.*, vol. 7, no. 4, pp. 262–266, Apr. 2016.

[28] G. Chen, T. M. Paronyan, E. M. Pigos, and A. R. Harutyunyan, "Enhanced gas sensing in pristine carbon nanotubes under continuous ultraviolet light illumination," *Sci. Rep.*, vol. 2, p. 343, Mar. 2012.

[29] J. Li, Y. Lu, Q. Ye, M. Cinke, J. Han, and M. Meyyappan, "Carbon nanotube sensors for gas and organic vapor detection," *Nano Lett.*, vol. 3, no. 7, pp. 929–933, Jul. 2003.

[30] W.-S. Cho, S.-I. Moon, K.-K. Paek, Y.-H. Lee, J.-H. Park, and B.-K. Ju, "Patterned multiwall carbon nanotube films as materials of NO_2 gas sensors," *Sensors Actuators B Chem.*, vol. 119, no. 1, pp. 180–185, Nov. 2006.

[31] T. Ueda, M. M. H. Bhuiyan, H. Norimatsu, S. Katsuki, T. Ikegami, and F. Mitsugi, "Development of carbon nanotube-based gas sensors for NO_x gas detection working at low temperature," *Physica E Low Dimensional Syst. Nanostruct.*, vol. 40, no. 7, pp. 2272–2277, May 2008.

[32] S. I. Moon *et al.*, "Bias-heating recovery of MWCNT gas sensor," *Mater. Lett.*, vol. 62, no. 16, pp. 2422–2425, Jun. 2008.

[33] *Spartan-6 FPGA Data Sheet: DC and Switching Characteristics (V3.1.1)*, Xilinx Inc., San Jose, CA, USA, Jan. 2015.

[34] *Cyclone II Device Handbook*, vol. 1, Altera Corporat., San Jose, CA, USA, 2008.

Encarnación Castillo received the M.Sc. and Ph.D. degrees in electronic engineering from the University of Granada, Granada, Spain, in 2002 and 2008, respectively.

From 2003 to 2005, she was a Research Fellow with the Department of Electronics and Computer Technology, University of Granada, where she is currently an Associate Professor. During her research fellowship, she carried out part of her research with the Department of Electrical and Computer Engineering, Florida State University, Tallahassee, FL, USA. She has authored over 50 technical papers in international journals and conferences. Her current research interests include the protection of IP protection of very large-scale integration (VLSI) and field-programmable gate arrays-based systems, as well as residue number system arithmetic, VLSI and FPL signal processing systems, and the combination of digital and analog programmable technologies for smart instrumentation for biosignal processing.

Dr. Castillo also serves regularly as a reviewer for IEEE journals.
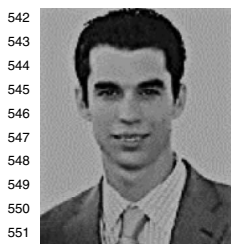
José F. Salmerón received the degrees in telecommunication engineering and electronics engineering from the University of Granada, Granada, Spain, in 2009 and 2011, respectively, and the master's degree in computer and network engineering and the Ph.D. degree in development of sensing capabilities in RFID technologies from the Technical University of Berlin, Berlin, Germany, in 2012 and 2014, respectively.

He is currently a Post-Doctoral Researcher with the Institute for Nanoelectronics, Technical University of Munich, Munich, Germany, where he is involved in the design and development of smart RFID labels with sensing capabilities.

Aniello Falco received the B.Sc. and M.Sc. degrees in electrical engineering from the University of Salerno, Salerno, Italy, in 2010 and 2013, respectively, and the Ph.D. degree from the Technical University of Munich, Munich, Germany, under the supervision of Prof. P. Lugli.

In 2013, he joined the Institute for Nanoelectronics, Technical University of Munich, where he conducted research on the solution processing of nanomaterials, for biological and sensing applications. Then, he moved to the Free University of Bozen-Bolzano, Bolzano, Italy, where he collaborated with his former supervisor to setup and develop a new research group on printed electronics.

Florin C. Loghin received the M.Sc. degree in electronic engineering from the Technical University of Munich, Munich, Germany, in 2015, where he is currently pursuing the Ph.D. degree with the Institute for Nanoelectronics.

His current research interests include the developing of carbon nanotube-based thin-film transistors and solution-processable-based organic electronics.

Francisco J. Romero received the B.Eng. degree (with valedictorian mention) in telecommunication engineering and the M.Eng. degree in telecommunications engineering from the University of Granada, Granada, Spain, in 2016 and 2018, respectively, where he is currently pursuing the Ph.D. degree with a national predoctoral scholarship.

In 2015, he joined the Department of Electronics and Computer Technology, University of Granada as an Ungraduated Researcher. His current research interests include graphene-based sensors, flexible electronics, and IoT embedded systems.

Paolo Lugli received the degree in physics from the University of Modena, Modena, Italy, in 1979, and the M.Sc. and Ph.D. degrees in electrical engineering from Colorado State University, Fort Collins, CO, USA, in 1982 and 1985, respectively.

He is currently the President of the Free University of Bozen-Bolzano, Bolzano, Italy. He has authored over 350 scientific papers.

Diego P. Morales received the M.Sc. degree in electronic engineering and the Ph.D. degree in electronic engineering from the University of Granada, Granada, Spain, in 2001 and 2011, respectively.

He was an Associate Professor with the Department of Computer Architecture and Electronics, University of Almería, Almería, Spain. He joined the Department of Electronics and Computer Technology, University of Granada, where he currently serves as a Tenured Professor. His current research interest includes developing reconfigurable applications.

Almudena Rivadeneyra received the master's degrees in telecommunication engineering, environmental sciences, and electronics engineering and the Ph.D. degree in design and development of environmental sensors from the University of Granada, Granada, Spain, in 2009, 2009, 2012, and 2014, respectively.

Since 2015, she has been with the Institute for Nanoelectronics, Technical University of Munich, Munich, Germany, where her research is centered in printed and flexible electronics with a special focus on sensors and RFID technology.